CMS Physics Analysis Summary

Contact: cms-pag-conveners-exotica@cern.ch 2015/07/07

Search for R-parity violating decays of scalar top quarks in events with two leptons, several jets, and low missing transverse momentum in pp collisions at 8 TeV

The CMS Collaboration

Abstract

The results of a search for top squark pair production in proton-proton collisions at $\sqrt{s} = 8$ TeV are presented. The search focuses on R-parity violating chargino-mediated decays of the top squark in final states with low missing transverse momentum, two opposite charge electrons or muons, and at least five jets. The analysis is based on a data sample corresponding to an integrated luminosity of 19.7 fb^{-1} collected with the CMS detector at the LHC in 2012. The data are found to be in agreement with the standard model expectation, and upper limits are placed on the top squark pair production cross section at the 95% confidence level. Top squark masses less than 1000 (890) GeV for the muon (electron) channel are excluded in models with a single non-zero coupling λ'_{ijk} $(i, j, k \leq 2)$.

1 Introduction

Supersymmetry [1, 2] (SUSY) is an extension of the standard model (SM) that provides a natural solution to the hierarchy problem [3, 4]. In the SUSY framework, quadratically divergent radiative corrections to the Higgs boson mass, dominated by loops involving the top quark, are canceled by loops with a scalar top partner (top squark). To avoid fine tuning, the mass of the top squark is expected to be not very different from the mass of the top quark, and the supersymmetric Higgs partners must not be too heavy [5, 6].

Searches for natural SUSY are carried out in many decay channels and can be divided into R-parity conserving (RPC) and R-parity violating (RPV) scenarios, where R-parity is a quantum number that is +1 for SM particles and -1 for superpartners [7]. In RPC models the top squark is expected to decay into the lightest supersymmetric particle (LSP) that escapes detection and results in an event signature with substantial missing transverse momentum $\vec{p}_{\mathrm{T}}^{\,\mathrm{miss}}$. Recent searches performed at the Large Hadron Collider (LHC) using events with high $\vec{p}_{\mathrm{T}}^{\,\mathrm{miss}}$ have set stringent lower bounds on the mass of the top squark [8–13]. If R-parity is not conserved, the LSP can decay to SM particles without substantial $\vec{p}_{\mathrm{T}}^{\,\mathrm{miss}}$. This motivates the search in events with low missing transverse momentum.

The superpotential terms that result in R-parity violation can be characterized by three trilinear Yukawa couplings λ_{ijk}, λ'_{ijk}, and λ''_{ijk}:

$$W_{\mathrm{RPV}} = \frac{1}{2}\lambda_{ijk}L_iL_j\overline{E}_k + \lambda'_{ijk}L_iQ_j\overline{D}_k + \frac{1}{2}\lambda''_{ijk}\overline{U}_i\overline{D}_j\overline{D}_k + \mu_iL_iH_u \tag{1}$$

where i, j, and k are generation indices; L and Q are the $SU(2)_L$ doublet superfields of the lepton and quark; and $\overline{E}$, $\overline{D}$, and $\overline{U}$ are the $SU(2)_L$ singlet superfields of the charged lepton, down-type quark, and up-type quark. The third term violates the conservation of baryon number, while the first two violate the conservation of lepton number. If both the baryon number and the lepton number are violated at the same time, this can lead to rapid proton decay, excluded by experimental observations [7]. For this reason and in order to simplify the interpretation of results, in this analysis we assume that only one of the λ'_{ijk} couplings is different from zero.

In SUSY models with the chargino $\tilde{\chi}^{\pm}$ lighter than a top squark and non-zero λ'_{ijk}, the top squark $\tilde{\mathrm{t}}$ can decay as $\tilde{\mathrm{t}} \to \mathrm{b}\tilde{\chi}^{\pm}$ with subsequent $\tilde{\chi}^{\pm}$ decay to a lepton and two jets via an off-shell sneutrino ($\tilde{\chi}^{\pm} \to l^{\pm}jj$) [14], as depicted in Fig. 1. The decay $\tilde{\chi}^{\pm} \to \nu$+jj via an off-shell slepton will also be non-negligible if the slepton and sneutrino masses are comparable.

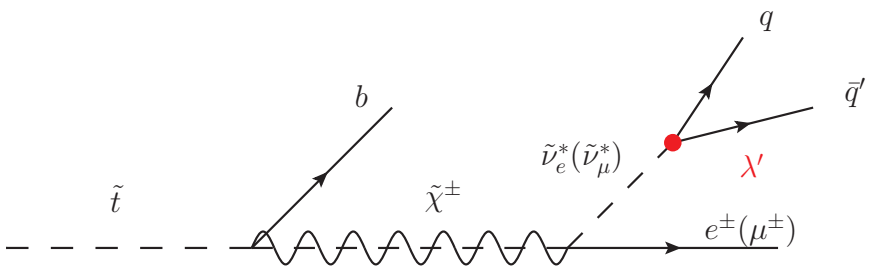

Figure 1: Diagram for the R-parity violating, chargino-mediated decay of a top squark. The chargino decays to a lepton and two jets via an off-shell sneutrino and non-zero λ'_{ijk}.

At the LHC top squarks are mainly produced in pairs. Thus, considering the first scenario, the search is performed using events with opposite sign muon ($\mu^{\pm}\mu^{\mp}$) or electron ($\mathrm{e}^{\pm}\mathrm{e}^{\mp}$) pairs, and at least five jets with at least one jet identified as arising from hadronization of a b quark

(b-tagged jet). The $\mu^{\pm}\mu^{\mp}$selection is equally sensitive to the RPV couplings λ'_{211}, λ'_{212}, λ'_{221}, λ'_{222}, and the $e^{\pm}e^{\mp}$selection to the RPV couplings λ'_{111}, λ'_{112}, λ'_{121}, λ'_{122}, respectively.

Other RPV SUSY searches via LQD coupling at LHC exist for several different models and final states. This includes several CMS [15–20] and ATLAS [21–24] searches, where mostly the new physics signatures are direct squarks decays into multiple leptons. The search in this article considers signature from top squarks undergoing a chargino-mediated decay involving the R-parity violating coupling, and complements the only search by CMS [18], where couplings to third generation, λ'_{3jk} were considered.

2 CMS detector

A description of the CMS detector, together with a definition of the coordinate system used and the relevant kinematic variables, can be found elsewhere [25]. A characteristic feature of the CMS detector is its superconducting solenoid magnet, of 6 m internal diameter, which provides a field of 3.8 T. Within the field volume are a silicon pixel and strip tracker, a lead tungstate crystal electromagnetic calorimeter (ECAL), and a brass and scintillator hadron calorimeter (HCAL). Muon detectors based on gas ionization chambers are embedded in a steel flux return yoke located outside the solenoid. Events are collected by a two-layer trigger system based on a hardware level 1 trigger (L1), followed by a software-based high level trigger (HLT).

The tracking system covers the pseudorapidity region $|\eta| < 2.5$, the muon detector $|\eta| < 2.4$, and the calorimeters $|\eta| < 3.0$. Additionally, the forward region at $3 < |\eta| < 5$ is covered by the steel and quartz fiber forward calorimeters. The near hermeticity of the detector permits accurate measurement of the energy balance in the transverse plane.

3 Simulation of background and signal events

Monte Carlo (MC) simulations of signal and background events were used to optimize selection criteria for maximum signal sensitivity and to estimate some backgrounds. The simulation of the hard scattering event was performed using the leading-order (LO) matrix-element event generator MADGRAPH5 [26], unless noted otherwise. The CTEQ6L1 [27] set of parton distribution functions (PDFs) with parameters based on measurements from the LHC run at $\sqrt{s}$ =7 TeV is used to describe the proton structure.

The simulation of the hard scattering event was then passed to PYTHIA 6.426 [28] with the Z2* tune [29] to model the parton shower, hadronization, multiple-parton interactions (MPI), and the underlying event. A full simulation of the interaction of stable particles with the CMS detector was performed using GEANT4 [30]. To reproduce the effect of multiple proton proton (pp) collisions per bunch crossing (pileup), a set of simulated events were mixed into the simulation of the hard scattering event.

The $t\bar{t}$ sample was generated with up to three additional partons, the Drell-Yan (DY) sample was produced with up to four additional partons, and the diboson (ZZ, WW, and WZ) samples were generated with up to two additional partons. POWHEG v1.0 [31–35] was used to simulate single top quark decays (*t*-, *s*-, and tW-channels). Simulated samples of $t\bar{t}$ and DY were normalized using cross sections computed at next-to-next-to-leading-order accuracy (NNLO) [36, 37]. Cross sections computed at next-to-leading order (NLO) accuracy [38, 39] are used to normalize single top quark and diboson samples.

The signal samples were also generated using MADGRAPH5 [26], PYTHIA 6.426 [28] and the

CTEQ6L1 PDF set. To normalize the signal samples, the top squark pair production cross section was computed as a function of the top squark mass $M_{\tilde{t}}$ at NLO accuracy, including soft gluon resummation at next-to-leading logarithmic (NLL) accuracy [40–43]. The uncertainty on the cross section includes the effect of the renormalization scale, factorization scale, and the PDF set [44].

4 Data, trigger, and object selection

The search is performed using $\sqrt{s} = 8$ TeV pp collisions corresponding to an integrated luminosity of 19.7 fb^{-1} collected by the CMS detector at the LHC in 2012. Events are selected using a trigger that requires at least one muon (electron) with a transverse momentum (p_{T}) threshold of 24 (27) GeV, and $|\eta| < 2.1$ (2.5). Data and simulated events are reconstructed using the same algorithms. All objects except electrons are reconstructed using the particle-flow (PF) algorithm [45], which uses information from all subsystems to reconstruct muons, photons, charged hadrons, and neutral hadrons.

To reduce the background from jets containing leptons, we impose isolation constraints on the energy $E_{T,\text{cone}}$ from particle tracks or deposits in the calorimeter within a cone $\Delta R = \sqrt{(\Delta\eta)^2 + (\Delta\phi)^2} = 0.4$ (0.3) around the trajectory of the muon (electron). The energy from the reconstructed lepton and the average energy density from pileup collisions are subtracted from $E_{T,\text{cone}}$.

Muons are required to have $p_{\mathrm{T}} > 50$ GeV and $|\eta| < 2.1$. Cosmic ray muons are rejected by requiring that the transverse (longitudinal) impact parameter be less than 2 (5) mm relative to the primary vertex, defined as the vertex with the greatest sum of the p_{T}^2 from all tracks. Only muons with at least ten hits in the silicon strip tracker and at least one hit in the pixel detector are considered, which ensures a precise momentum measurement. Isolation is imposed by the requirement that $E_{T,\text{cone}}$ be less than 12% of the muon p_{T} [46]. The muon reconstruction and trigger efficiencies in simulation are scaled to match the measured efficiencies from data in bins of p_{T} and η.

Electrons are reconstructed by matching an energy cluster in the ECAL with a track reconstructed using a Gaussian sum filter [47]. Electrons are required to have $p_{\mathrm{T}} > 50$ GeV with $|\eta| < 2.5$ and the gap between the ECAL barrel and endcap excluded ($1.4442 < |\eta| < 1.5660$). Electrons are identified using a multivariate identification algorithm (MVA) [48]. Input variables are sensitive to bremsstrahlung along the electron path, matching between tracks and ECAL energy deposits and shower-shape variables. MVA training was performed on a sample of simulated DY events that contains true electrons and a data sample enriched in misidentified electrons. In addition, the transverse impact parameter is required to be less than 2 mm. To reduce backgrounds that arise from photon conversions in the inner pixel detector, at least one pixel hit in the innermost pixel layer is required and the electron must be inconsistent with photon pair production in the tracker. We ensure that the electron is isolated from other activity in the event by requiring that $E_{T,\text{cone}}$ be less than 10% of the electron p_{T} [49]. The differences in electron reconstruction and trigger efficiencies between data and simulation were corrected in simulation in bins of p_{T} and η.

Jets are reconstructed from PF objects [50] using the anti-k_{T} clustering algorithm [51] with a distance parameter of 0.5. Jets from potential instrumental and non-collision sources are eliminated by requiring the fraction of jet energy coming from charged and neutral electromagnetic deposits to be less than 0.99, the neutral hadron fraction to be less than 0.99, and the charged hadron fraction to be greater than zero. The energy and momentum of the jets are corrected as a

Table 1: Summary of signal and control samples, including selections on the dimuon (dielectron) mass $M_{\ell\ell}$. The samples $\mathrm{t\bar{t}}$, DY normalization, and DY shape are used in data-based procedures described below to estimate SM backgrounds in the search region.

Selection	Leptons	N_{jets}	$N_{\text{b-tags}}$
Search	$\mathrm{e^{\pm}e^{\mp}}(\mu^{\pm}\mu^{\mp})$ $M_{\ell\ell}$ >130 GeV	≥ 5	≥ 1
$\mathrm{t\bar{t}}$	$e^{\pm}\mu^{\mp}$	≥ 5	≥ 1
DY normalization	$\mathrm{e^{\pm}e^{\mp}}(\mu^{\pm}\mu^{\mp})$, $50 < M_{\ell\ell} < 130$ GeV	≥ 2	≥ 1
DY shape	$\mathrm{e^{\pm}e^{\mp}}(\mu^{\pm}\mu^{\mp})$, $50 < M_{\ell\ell} < 130$ GeV	≥ 2	0

function of the jet p_{T} and η to account for the nonlinear response of the calorimeter. The average energy from pileup is subtracted from the jet [52]. Only jets within the tracker fiducial volume are considered ($|\eta| < 2.4$). The jet p_{T} must be at least 100 GeV for the leading jet, 50 GeV for the second-leading jet, and 30 GeV for the remaining jets. Any jet reconstructed within $\Delta R < 0.5$ of a muon or electron is rejected. The combined secondary-vertex (CSV) algorithm [53] uses information from the track impact parameter and vertex information to discriminate between jets that originate from b quarks (b-tagged jets) and jets from light-flavor quarks and gluons. This procedure correctly identifies b-tagged jets with an efficiency of approximately 70% and misidentifies jets from light-flavor quarks or gluons at a rate of approximately 1% [53]. The efficiency in the simulation is scaled to match the measured efficiency in data as a function of p_{T}, η and flavor of the jet. Events are required to have at least one b-tagged jet.

The missing transverse momentum vector $\vec{p}_{\mathrm{T}}^{\,\mathrm{miss}}$ in the event is defined as the projection of the negative vector sum of the momenta of all reconstructed particles on the plane perpendicular to the beams. Its magnitude is referred to as $E_{\mathrm{T}}^{\mathrm{miss}}$ and is computed using PF objects. To suppress leptonic $\mathrm{t\bar{t}}$ decays that often have significant $E_{\mathrm{T}}^{\mathrm{miss}}$ due to the presence of neutrinos in the final state, we require $E_{\mathrm{T}}^{\mathrm{miss}}$ to be less than 100 GeV.

The dilepton pair must have opposite charge and same flavor. The dilepton mass $M_{\ell\ell}$, computed from the two lepton momenta, must be greater than 130 GeV to reduce the contribution from low-mass resonances and on-shell DY decays.

To enhance the statistical significance, the sample is divided into three exclusive categories of jet multiplicity N_{jets} (5, 6, ≥ 7) for each lepton flavor. The scalar sum of the transverse momenta S_{T} of jets and leptons in the event is used to improve the sensitivity to signal decays. We compute an S_{T} threshold $S_{\mathrm{T}}^{\mathrm{min}}$ optimized for each $M_{\tilde{\mathrm{t}}}$ hypothesis. $S_{\mathrm{T}}^{\mathrm{min}}$ is optimized independently for each N_{jets} category by maximizing the value of $S/\sqrt{S+B}$, where S is the number of expected signal events and B the number of background events above $S_{\mathrm{T}}^{\mathrm{min}}$. A summary of signal and control samples, including selections on the dilepton mass is described in Table 1.

5 Background estimation

All backgrounds are estimated from data using the control samples listed in Table 1, except for diboson and single top quark backgrounds, which we estimate from simulation. Simulated samples are reweighted so that the pileup distribution matches the measured pileup distribution in data. In simulated $\mathrm{t\bar{t}}$ events the top quark p_{T} is reweighted to match the measured differential cross section [54, 55].

The dominant background stems from leptonic $\mathrm{t\bar{t}}$ decays. The signal produces only same-flavor leptons, so we estimate the $\mathrm{t\bar{t}}$ background from a control sample of $\mathrm{e^{\pm}}\mu^{\mp}$events. We use this

control sample to compute a correction factor for the $t\bar{t}$ simulation in the signal region. The correction factor is defined as the ratio of the number of events in this background-subtracted data sample to the number of events expected from the simulated $t\bar{t}$ background. Simulated contributions from the DY, diboson, and single top quark backgrounds are subtracted. The $e^{\pm}\mu^{\mp}$control sample is well modeled by the simulation, and the obtained correction factors for different jet multiplicities are statistically consistent with unity.

DY decays constitute approximately 10% of the SM background in the signal region, and are reduced by requiring at least one b-tagged jet. The DY contribution is estimated using a control sample of two opposite charge same-flavor leptons, which have $M_{\ell\ell}$ in the range 50–130 GeV. We perform a fit to the $M_{\ell\ell}$ distribution to estimate the number of DY events. The DY shape is obtained from background-subtracted data using a DY-enriched sample with no b-tagged jets. The background from diboson decays including leptonic Z decays is estimated from simulation and is constrained in the fit. The $M_{\ell\ell}$ shape for remaining backgrounds does not exhibit a peak at the Z mass, and it is described by a first degree polynomial. The fit determines the number of DY events N_{DY}, and the number of background events. To check that the procedure is insensitive to the potential signal contribution, we performed a fit with signal events included, and observed that obtained N_{DY} is independent of the presence of the potential signal in the control sample. The ratio of N_{DY} from the fit to the simulated number of DY events is calculated per each N_{jets} bin and used to correct the simulation. This correction factor ranges from 1.16–2.11 and increases with jet multiplicity.

We checked that the corrections to the DY normalization are valid in the signal region with $M_{\ell\ell} > 130$ GeV. To demonstrate this, we compared the numbers of events in different mass ranges using a DY-enriched sample with at least five jets and no b-tagged jets. The ratio of events with $M_{\ell\ell}$ in the normalization region compared to the signal region was predicted from simulation to be 11.8, and found to be 14 ± 3.5 in data. The agreement suggests that the shape of the $M_{\ell\ell}$ distribution is well modeled by simulation.

6 Systematic uncertainties

We estimate systematic uncertainties for each background and the expected signal yield.

Since the top correction factor to the MC was estimated from a control sample of $e^{\pm}\mu^{\mp}$events in data, the systematic uncertainty on this background was determined by the statistical uncertainty on the control sample. This uncertainty ranges from 10–50%, depending on N_{jets} and the value of $S_{\mathrm{T}}^{\mathrm{min}}$. For the DY background, we take the scale correction obtained from the fit to data as the uncertainty. The uncertainty ranges from 8–100%, and is always larger than the statistical uncertainty from the fit.

We assign a conservative 30% uncertainty to the diboson and single top backgrounds contribution to account for the difference between the NLO theoretical calculation and the CMS measurement of the WW and ZZ cross sections [56] and single top cross sections [57, 58] respectively.

The statistical uncertainty due to the finite size of the simulated background samples is 10–30% depending on the N_{jets} bin and $S_{\mathrm{T}}^{\mathrm{min}}$ value.

The source of systematic uncertainties on the signal efficiency are consider to arise from the jet energy scale (5%) [52], b-tag jet efficiencies (3%), luminosity (2.6%) [59], lepton identification (3%), electron energy scale (2%), muon momentum scale (0.9%), and trigger (1%) where numbers in brakets correspond to 1σ uncertainties. For uncertainty on b-tagging efficiencies, the

efficiency and misidentification rates were varied by their uncertainties [60], and the effect on signal prediction was recorded. The uncertainty related to the lepton isolation requirement for signal events with many jets was estimated using a $t\bar{t}$ control sample with ≥ 7 jets, which is equal to 5%. The uncertainty due to the finite size of the simulated signal sample was 2–7%. The impact of the PDF set and pileup were determined to be negligible.

Tables 2 summarize the range of systematic uncertainties for signal and background.

Table 2: List of systematic uncertainties included in the likelihood fit on signal and background normalization.

Parameter type	Source	Uncertainty (%)
Background Normalization	$t\bar{t}$+jets	10-50
	Drell-Yan	50-100
	Diboson	30
	Single top	30
	MC statistics	10-30
Signal Efficiency	Jet energy scale	5
	b-tagging scale factor	1-3
	Luminosity	2.6
	Lepton id/reco	3
	Electron energy scale	2
	Muon momentum scale	0.9
	Trigger	1
	Lepton isolation	5
	MC statistics	2-7

7 Results

Distributions of jet multiplicity for data and expected background contributions from the $\mu^{\pm}\mu^{\mp}$ and $e^{\pm}e^{\mp}$selections are shown in Fig. 2. The numbers of observed events agree with the SM background expectations.

For each $M_{\tilde{t}}$ hypothesis an optimal S_T^{min} cut is found for each N_{jets} bin to maximize the sensitivity to the new physics signal. Tables 3 and 4 present the numbers of expected and observed events for different N_{jets} bins, along with the optimized value of S_T^{min}.

We use the modified frequentist CL_s method [61, 62] with a log likelihood test statistic to derive 95% confidence level (C.L.) limits on the top squark pair production cross section. For each $M_{\tilde{t}}$ hypothesis, the Poisson likelihoods of three N_{jets} bins are combined. Systematic uncertainties are incorporated into the test statistic as nuisance parameters. The nuisance parameter probability distribution function (pdf) for $t\bar{t}$ background normalization is described by a gamma function, while all other uncertainties are treated with log-normal pdfs. With an exception of uncertainties related to the finite size of a control sample, we conservatively assume that the systematic uncertainties are fully correlated across different N_{jets} bins.

The signal search regions, namely jet multiplicity distributions after S_T^{min} selection optimized for a $M_{\tilde{t}}$ hypothesis of 300 and 900 GeV are shown in Fig. 2. The new physics signal shown by a blue line is superimposed with the expected SM background. The statistical and systematic uncertainties for the SM contributions are shown with the hatched band at the upper plot

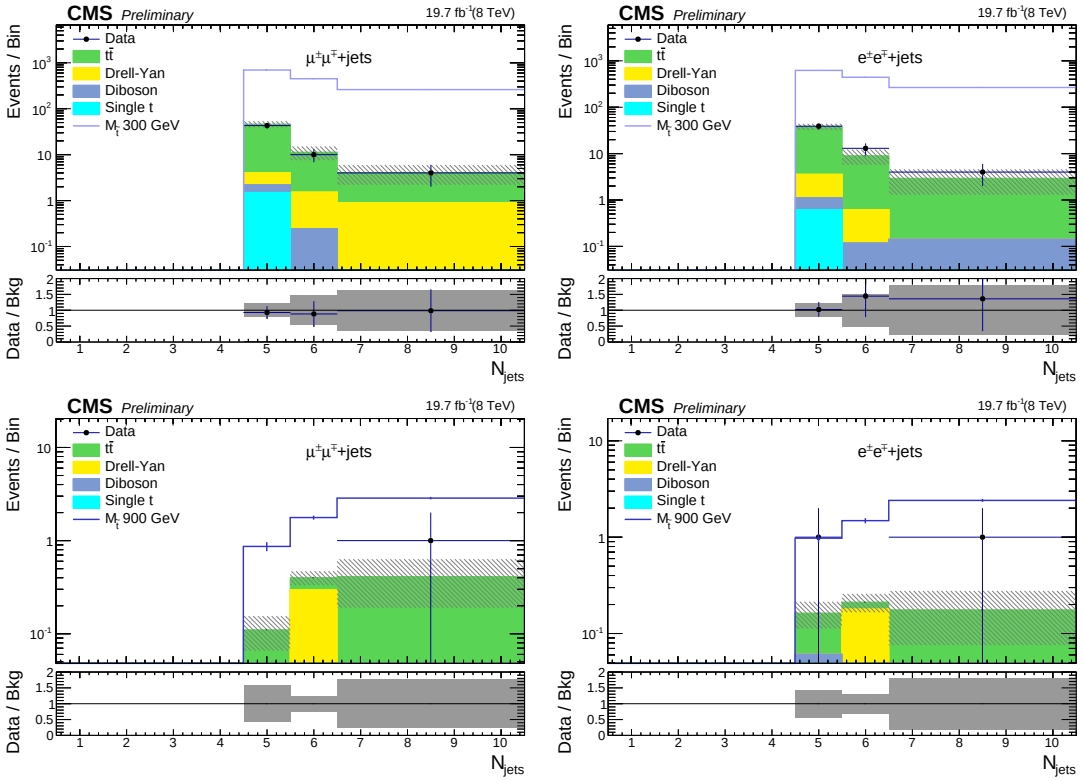

Figure 2: Jet multiplicity distribution for $\mu^{\pm}\mu^{\mp}$(left) and $e^{\pm}e^{\mp}$(right) after S_{T}^{min} selection optimized for a $M_{\tilde{t}}$ hypothesis of 300 and 900 GeV. The new physics signal shown by a blue line is superimposed with the expected SM background. The statistical and systematic uncertainties for the SM contributions are shown with the hatched band at the upper plot and with the grey band on the ratio plot below.

and with the grey band on the ratio plot below. Similar distributions for the signal inference are used for each of the other $M_{\tilde{t}}$ hypothesis. The NLO signal cross sections [44] are used to normalize the signal histograms.

The expected and observed limits on the top squark pair production cross section are shown in Fig. 3. The computed limits correspond to the scenario where only one of the λ'_{ijk} $(i, j, k \leq 2)$ couplings is different from zero, and are 1000 (890) GeV for the muon (electron) channel. The difference in $M_{\tilde{t}}$ and chargino mass $M_{\tilde{\chi}^{\pm}}$ is fixed at 100 GeV. The theory curve represents the NLO+NLL signal cross sections [44] for each $M_{\tilde{t}}$ hypothesis.

In Tables 3 and 4 we also present the observed and expected event yields from the SM backgrounds in different N_{jets} categories. From here the interpretation of results for a generic set of λ'_{ijk} couplings, $i, j, k = 3$ can be made, including scenarios with non-zero couplings to the third generation SM particles, where this analysis retains sensitivity through the leptonic τ decays.

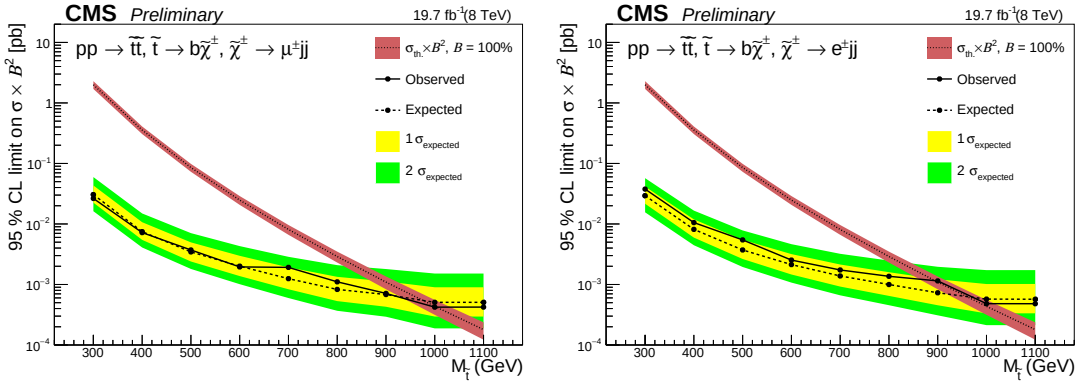

Figure 3: Observed and median expected cross section limits for $\mu^{\pm}\mu^{\mp}$(left) and $e^{\pm}e^{\mp}$(right). The bands denoted 1σ and 2σ correspond to the change in the expected limit as the uncertainties are varied by 1-2 σ. The theory cross section line shows the expected top squark cross section computed at NLO+NLL [40–43].

8 Summary

We perform a search for new phenomena using events with two opposite sign muons or electrons, at least five jets, at least one b-tagged jet, and low $E_{\text{T}}^{\text{miss}}$. No excess over the expected background is observed, and the data are interpreted in the framework of chargino-mediated, RPV top squark decays. In models with a single non-zero λ'_{ijk} $(i, j, k \leq 2)$, the results exclude top squarks with mass less than 1000 (890) GeV for the muon (electron) channel at the 95% confidence level. The expected limits are 970 (950) GeV for the muon (electron) channel. These limits, which are the first for this model, are complementary to published limits on chargino-mediate, RPV top squark decays via non-zero λ'_{3jk} [18].

Table 3: Observed, expected background and signal event yields in 5, 6, and ≥ 7 jet bins, for different top squark masses using $\mu^{\pm}\mu^{\mp}$selection. The uncertainty on the expected background is the total systematic uncertainty.

Mass (GeV)	N_{jets}	$S_{\text{T}}^{\text{min}}$ (GeV)	Data	Expected background	Signal
300	5	475	43	46.3 ± 7.2	696.0 ± 52.4
300	6	475	10	11.3 ± 3.8	450.2 ± 42.5
300	≥ 7	325	4	4.1 ± 1.9	261.0 ± 32.6
400	5	525	39	36.8 ± 7.2	266.4 ± 13.5
400	6	525	10	10.8 ± 3.9	280.9 ± 14.1
400	≥ 7	325	4	4.1 ± 1.9	222.6 ± 12.4
500	5	725	16	16.0 ± 3.8	81.1 ± 4.0
500	6	675	9	7.3 ± 3.2	114.4 ± 4.8
500	≥ 7	675	3	3.1 ± 1.6	101.8 ± 4.5
600	5	875	5	5.2 ± 1.5	23.6 ± 1.1
600	6	825	5	4.6 ± 1.6	36.0 ± 1.3
600	≥ 7	825	2	2.3 ± 1.0	44.2 ± 1.5
700	5	1075	2	1.3 ± 0.4	7.7 ± 0.4
700	6	975	4	2.4 ± 0.8	13.2 ± 0.5
700	≥ 7	975	2	1.0 ± 0.5	17.8 ± 0.5
800	5	1175	0	0.9 ± 0.3	2.9 ± 0.2
800	6	1175	2	0.8 ± 0.3	4.5 ± 0.2
800	≥ 7	1125	1	0.4 ± 0.2	7.3 ± 0.2
900	5	1475	0	0.1 ± 0.1	0.9 ± 0.1
900	6	1325	0	0.4 ± 0.2	1.8 ± 0.1
900	≥ 7	1175	1	0.4 ± 0.2	2.9 ± 0.1
1000	5	1575	0	0.1 ± 0.1	0.4 ± 0.1
1000	6	1525	0	< 0.1	0.6 ± 0.1
1000	≥ 7	1425	0	0.2 ± 0.2	1.2 ± 0.1

Table 4: Observed, expected background and signal event yields in 5, 6, and ≥ 7 jet bins, for different top squark masses using $e^{\pm}e^{\mp}$selection. The uncertainty on the expected background is the total systematic uncertainty.

Mass (GeV)	N_{jets}	$S_{\text{T}}^{\text{min}}$ (GeV)	Data	Expected background	Signal
300	5	325	39	38.1 ± 5.9	621.8 ± 49.1
300	6	325	13	9.0 ± 3.3	442.0 ± 41.1
300	≥ 7	325	4	2.9 ± 1.7	266.2 ± 32.9
400	5	525	27	28.7 ± 5.6	256.3 ± 13.6
400	6	325	13	9.0 ± 3.3	245.5 ± 13.1
400	≥ 7	325	4	2.9 ± 1.7	180.5 ± 11.5
500	5	725	12	14.1 ± 3.3	69.2 ± 3.3
500	6	675	9	5.3 ± 2.5	88.1 ± 3.8
500	≥ 7	675	4	2.2 ± 1.4	89.7 ± 3.8
600	5	925	1	3.4 ± 1.1	19.0 ± 0.9
600	6	875	3	2.7 ± 1.0	28.8 ± 1.2
600	≥ 7	825	4	1.8 ± 0.9	38.7 ± 1.3
700	5	1025	1	1.6 ± 0.5	7.1 ± 0.3
700	6	975	2	1.3 ± 0.5	10.5 ± 0.4
700	≥ 7	975	2	1.1 ± 0.6	14.8 ± 0.5
800	5	1225	1	0.4 ± 0.2	2.7 ± 0.2
800	6	1175	0	0.4 ± 0.2	3.6 ± 0.2
800	≥ 7	1075	2	0.7 ± 0.4	5.7 ± 0.2
900	5	1325	1	0.2 ± 0.1	1.0 ± 0.1
900	6	1375	0	0.2 ± 0.1	1.5 ± 0.1
900	≥ 7	1375	1	0.2 ± 0.1	2.4 ± 0.1
1000	5	1475	0	0.1 ± 0.1	0.3 ± 0.1
1000	6	1425	0	0.2 ± 0.1	0.6 ± 0.1
1000	≥ 7	1525	0	0.1 ± 0.1	1.0 ± 0.1

Acknowledgements

We congratulate our colleagues in the CERN accelerator departments for the excellent performance of the LHC and thank the technical and administrative staffs at CERN and at other CMS institutes for their contributions to the success of the CMS effort. In addition, we gratefully acknowledge the computing centres and personnel of the Worldwide LHC Computing Grid for delivering so effectively the computing infrastructure essential to our analyses. Finally, we acknowledge the enduring support for the construction and operation of the LHC and the CMS detector provided by the following funding agencies: BMWFW and FWF (Austria); FNRS and FWO (Belgium); CNPq, CAPES, FAPERJ, and FAPESP (Brazil); MES (Bulgaria); CERN; CAS, MoST, and NSFC (China); COLCIENCIAS (Colombia); MSES and CSF (Croatia); RPF (Cyprus); MoER, ERC IUT and ERDF (Estonia); Academy of Finland, MEC, and HIP (Finland); CEA and CNRS/IN2P3 (France); BMBF, DFG, and HGF (Germany); GSRT (Greece); OTKA and NIH (Hungary); DAE and DST (India); IPM (Iran); SFI (Ireland); INFN (Italy); NRF and WCU (Republic of Korea); LAS (Lithuania); MOE and UM (Malaysia); CINVESTAV, CONACYT, SEP, and UASLP-FAI (Mexico); MBIE (New Zealand); PAEC (Pakistan); MSHE and NSC (Poland); FCT (Portugal); JINR (Dubna); MON, RosAtom, RAS and RFBR (Russia); MESTD (Serbia); SEIDI and CPAN (Spain); Swiss Funding Agencies (Switzerland); MST (Taipei); ThEPCenter, IPST, STAR and NSTDA (Thailand); TUBITAK and TAEK (Turkey); NASU and SFFR (Ukraine); STFC (United Kingdom); DOE and NSF (USA).

Individuals have received support from the Marie-Curie programme and the European Research Council and EPLANET (European Union); the Leventis Foundation; the A. P. Sloan Foundation; the Alexander von Humboldt Foundation; the Belgian Federal Science Policy Office; the Fonds pour la Formation à la Recherche dans l'Industrie et dans l'Agriculture (FRIA-Belgium); the Agentschap voor Innovatie door Wetenschap en Technologie (IWT-Belgium); the Ministry of Education, Youth and Sports (MEYS) of the Czech Republic; the Council of Science and Industrial Research, India; the HOMING PLUS programme of Foundation for Polish Science, cofinanced from European Union, Regional Development Fund; the Compagnia di San Paolo (Torino); the Consorzio per la Fisica (Trieste); MIUR project 20108T4XTM (Italy); the Thalis and Aristeia programmes cofinanced by EU-ESF and the Greek NSRF; and the National Priorities Research Program by Qatar National Research Fund.

References

[1] P. Fayet and S. Ferrara, "Supersymmetry", *Phys. Rept.* **32** (1977) 249, doi:10.1016/0370-1573(77)90066-7.

[2] S. P. Martin, "A Supersymmetry primer", *Adv. Ser. Direct. High Energy Phys.* **21** (2010) 1, doi:10.1142/9789814307505_0001, arXiv:hep-ph/9709356.

[3] S. Dimopoulos and G. Giudice, "Naturalness constraints in supersymmetric theories with nonuniversal soft terms", *Phys. Lett. B* **357** (1995) 573–578, doi:10.1016/0370-2693(95)00961-J, arXiv:hep-ph/9507282.

[4] B. de Carlos and J. Casas, "One loop analysis of the electroweak breaking in supersymmetric models and the fine tuning problem", *Phys. Lett. B* **309** (1993) 320–328, doi:10.1016/0370-2693(93)90940-J, arXiv:hep-ph/9303291.

[5] M. Papucci, J. T. Ruderman, and A. Weiler, "Natural SUSY Endures", *JHEP* **1209** (2012) 035, doi:10.1007/JHEP09(2012)035, arXiv:1110.6926.

[6] R. Kitano and Y. Nomura, "Supersymmetry, naturalness, and signatures at the LHC", *Phys. Rev. D* **73** (2006) 095004, doi:10.1103/PhysRevD.73.095004, arXiv:hep-ph/0602096.

[7] R. Barbier et al., "*R*-parity violating supersymmetry", *Phys. Rept.* **420** (2005) 1, doi:10.1016/j.physrep.2005.08.006, arXiv:hep-ph/0406039.

[8] CMS Collaboration, "Search for top squark and higgsino production using diphoton Higgs boson decays", *Phys. Rev. Lett.* **112** (2014) 161802, doi:10.1103/PhysRevLett.112.161802, arXiv:1312.3310.

[9] CMS Collaboration, "Search for top-squark pairs decaying into Higgs or Z bosons in pp collisions at $\sqrt{s}$ = 8 TeV", *Phys. Lett. B* **736** (2014) 371–397, doi:10.1016/j.physletb.2014.07.053, arXiv:1405.3886.

[10] CMS Collaboration, "Search for top-squark pair production in the single-lepton final state in pp collisions at $\sqrt{s}$ = 8 TeV", *Eur. Phys. J. C* **73** (2013) 2677, doi:10.1140/epjc/s10052-013-2677-2, arXiv:1308.1586.

[11] ATLAS Collaboration, "Search for direct pair production of the top squark in all-hadronic final states in proton-proton collisions at $\sqrt{s}$ = 8 TeV with the ATLAS detector", *JHEP* **1409** (2014) 015, doi:10.1007/JHEP09(2014)015, arXiv:1406.1122.

[12] ATLAS Collaboration, "Search for direct top-squark pair production in final states with two leptons in pp collisions at $\sqrt{s}$ = 8 TeV with the ATLAS detector", *JHEP* **1406** (2014) 124, doi:10.1007/JHEP06(2014)124, arXiv:1403.4853.

[13] ATLAS Collaboration, "Search for top squark pair production in final states with one isolated lepton, jets, and missing transverse momentum in $\sqrt{s}$ = 8 TeV pp collisions with the ATLAS detector", *JHEP* **1411** (2014) 118, doi:10.1007/JHEP11(2014)118, arXiv:1407.0583.

[14] J. A. Evans and Y. Kats, "LHC Coverage of RPV MSSM with Light Stops", *JHEP* **1304** (2013) 028, doi:10.1007/JHEP04(2013)028, arXiv:1209.0764.

[15] CMS Collaboration, "Search for RPV supersymmetry with three or more leptons and b-tags", CMS Physics Analysis Summary CMS-PAS-SUS-12-027, CERN, 2012.

[16] CMS Collaboration, "Search for RPV SUSY in the four-lepton final state", CMS Physics Analysis Summary CMS-PAS-SUS-13-010, CERN, 2013.

[17] CMS Collaboration, "Search for RPV SUSY resonant second generation slepton production in same-sign dimuon events at $\sqrt{s}$ = 7 TeV", CMS Physics Analysis Summary CMS-PAS-SUS-13-005, CERN, 2013.

[18] CMS Collaboration, "Search for pair production of third-generation scalar leptoquarks and top squarks in proton-proton collisions at $\sqrt{s}$ = 8 TeV", *Phys. Lett. B* **739** (2014) 229, doi:10.1016/j.physletb.2014.10.063, arXiv:1408.0806.

[19] CMS Collaboration, "Search for lepton flavour violating decays of heavy resonances and quantumblack holes to e/mu pairs in pp collisions at $\sqrt{s}$ = 8 TeV", Technical Report CMS-PAS-EXO-13-002, CERN, 2015.

[20] CMS Collaboration, "Search for top squarks in R-parity-violating supersymmetry using three or more leptons and b-tagged jets", *Phys. Rev. Lett.* **111** (2013) 221801, doi:10.1103/PhysRevLett.111.221801, arXiv:1306.6643.

[21] ATLAS Collaboration, "Search for a heavy neutral particle decaying to eμ, eτ, or $\mu\tau$ in ppcollisions $\sqrt{s}$ = 8 TeV with the ATLAS detector", arXiv:1503.04430. Submitted to *Phys. Rev. Lett*.

[22] ATLAS Collaboration, "Search for long-lived, heavy particles in final states with a muon and a multi-track displaced vertex in proton-proton collisions at $\sqrt{s}$ = 8 TeV with the ATLAS detector", Technical Report ATLAS-CONF-2013-092, CERN, 2013.

[23] ATLAS Collaboration, "A search for $B - L$ R-Parity violating scalar top decays in $\sqrt{s}$ = 8 TeV pp collisions with the ATLAS experiment", Technical Report ATLAS-CONF-2015-015, CERN, Mar, 2015.

[24] ATLAS Collaboration, "Constraints on promptly decaying supersymmetric particles with lepton-number- and R-parity-violating interactions using Run-1 ATLAS data", Technical Report ATLAS-CONF-2015-018, CERN, 2015.

[25] CMS Collaboration, "The CMS experiment at the CERN LHC", *JINST* **3** (2008) S08004, doi:10.1088/1748-0221/3/08/S08004.

[26] J. Alwall et al., "MadGraph 5: going beyond", *JHEP* **06** (2011) 128, doi:10.1007/JHEP06(2011)128, arXiv:1106.0522.

[27] J. Pumplin et al., "New generation of parton distributions with uncertainties from global QCD analysis", *JHEP* **07** (2002) 012, doi:10.1088/1126-6708/2002/07/012, arXiv:hep-ph/0201195.

[28] T. Sjöstrand, S. Mrenna, and P. Skands, "PYTHIA 6.4 physics and manual", *JHEP* **05** (2006) 26, doi:10.1088/1126-6708/2006/05/026, arXiv:hep-ph/0603175.

[29] CMS Collaboration, "Study of the underlying event at forward rapidity in pp collisions at $\sqrt{s}$ = 0.9, 2.76, and 7 TeV", *JHEP* **1304** (2013) 072, doi:10.1007/JHEP04(2013)072, arXiv:1302.2394.

[30] GEANT4 Collaboration, "GEANT4 – a simulation toolkit", *Nucl. Instrum. Meth. A* **506** (2003) 250, doi:10.1016/S0168-9002(03)01368-8.

[31] S. Alioli, P. Nason, C. Oleari, and E. Re, "NLO single-top production matched with shower in POWHEG: s- and t-channel contributions", *JHEP* **09** (2009) 111, doi:10.1088/1126-6708/2009/09/111, arXiv:0907.4076. [Erratum: doi:10.1007/JHEP02(2010)011].

[32] E. Re, "Single-top Wt-channel production matched with parton showers using the POWHEG method", *Eur. Phys. J. C* **71** (2011) 1547, doi:10.1140/epjc/s10052-011-1547-z, arXiv:1009.2450.

[33] P. Nason, "A New method for combining NLO QCD with shower Monte Carlo algorithms", *JHEP* **11** (2004) 040, doi:10.1088/1126-6708/2004/11/040, arXiv:hep-ph/0409146.

[34] S. Frixione, P. Nason, and C. Oleari, "Matching NLO QCD computations with Parton Shower simulations: the POWHEG method", *JHEP* **11** (2007) 070, doi:10.1088/1126-6708/2007/11/070, arXiv:0709.2092.

[35] S. Alioli, P. Nason, C. Oleari, and E. Re, "A general framework for implementing NLO calculations in shower Monte Carlo programs: the POWHEG BOX", *JHEP* **06** (2010) 043, doi:10.1007/JHEP06(2010)043, arXiv:1002.2581.

[36] M. Czakon, P. Fiedler, and A. Mitov, "Total Top-Quark Pair-Production Cross Section at Hadron Colliders Through $O(\alpha_S^4)$", *Phys. Rev. Lett.* **110** (2013) 252004, doi:10.1103/PhysRevLett.110.252004, arXiv:1303.6254.

[37] R. Gavin, Y. Li, F. Petriello, and S. Quackenbush, "FEWZ 2.0: A code for hadronic Z production at next-to-next-to-leading order", *Comput. Phys. Commun.* **182** (2011) 2388, doi:10.1016/j.cpc.2011.06.008, arXiv:1011.3540.

[38] N. Kidonakis and R. Vogt, "Theoretical top quark cross section at the Tevatron and the LHC", *Phys. Rev. D* **78** (2008) 074005, doi:10.1103/PhysRevD.78.074005, arXiv:0805.3844.

[39] J. M. Campbell, R. K. Ellis, and C. Williams, "Vector boson pair production at the LHC", *JHEP* **07** (2011) 018, doi:10.1007/JHEP07(2011)018, arXiv:1105.0020.

[40] W. Beenakker, R. Hopker, M. Spira, and P. Zerwas, "Squark and gluino production at hadron colliders", *Nucl. Phys. B* **492** (1997) 51, doi:10.1016/S0550-3213(97)80027-2, arXiv:hep-ph/9610490.

[41] A. Kulesza and L. Motyka, "Threshold resummation for squark-antisquark and gluino-pair production at the LHC", *Phys. Rev. Lett.* **102** (2009) 111802, doi:10.1103/PhysRevLett.102.111802, arXiv:0807.2405.

[42] A. Kulesza and L. Motyka, "Soft gluon resummation for the production of gluino-gluino and squark-antisquark pairs at the LHC", *Phys. Rev. D* **80** (2009) 095004, doi:10.1103/PhysRevD.80.095004, arXiv:0905.4749.

[43] W. Beenakker et al., "Soft-gluon resummation for squark and gluino hadroproduction", *JHEP* **12** (2009) 041, doi:10.1088/1126-6708/2009/12/041, arXiv:0909.4418.

[44] M. Krämer et al., "Supersymmetry production cross sections in pp collisions at $\sqrt{s} = 7$ TeV", (2012). arXiv:1206.2892. CERN-PH-TH/2012-163.

[45] CMS Collaboration, "Commissioning of the Particle-flow Event Reconstruction with the first LHC collisions recorded in the CMS detector", CMS Physics Analysis Summary CMS-PAS-PFT-10-001, CERN, 2010.

[46] CMS Collaboration, "Performance of CMS muon reconstruction in pp Collisions at $\sqrt{s} =$ 7 TeV", *JINST* **7** (2012) 10002, doi:10.1088/1748-0221/7/10/P10002, arXiv:1206.4071.

[47] CMS Collaboration, "Electron reconstruction and identification at $\sqrt{s} = 7$ TeV", CMS Physics Analysis Summary CMS-PAS-EGM-10-004, CERN, 2010.

[48] CMS Collaboration, "Performance of electron reconstruction and selection with the CMS detector in proton-proton collisions at $\sqrt{s} = 8$ TeV", arXiv:1502.02701. Submitted to *JINST*.

[49] CMS Collaboration, "Particle-flow commissioning with muons and electrons from J/ψ and W events at 7 TeV", CMS Physics Analysis Summary CMS-PAS-PFT-10-003, CERN, 2010.

[50] CMS Collaboration, "Particle-Flow Event Reconstruction in CMS and Performance for Jets, Taus, and MET", CMS Physics Analysis Summary CMS-PAS-PFT-09-001, CERN, 2009.

[51] M. Cacciari, G. P. Salam, and G. Soyez, "The Anti-k_t jet clustering algorithm", *JHEP* **04** (2008) 063, doi:10.1088/1126-6708/2008/04/063, arXiv:0802.1189.

[52] CMS Collaboration, "Determination of Jet Energy Calibration and Transverse Momentum Resolution in CMS", *JINST* **6** (2011) P11002, doi:10.1088/1748-0221/6/11/P11002, arXiv:1107.4277.

[53] CMS Collaboration, "Identification of b-quark jets with the CMS experiment", *JINST* **8** (2013) P04013, doi:10.1088/1748-0221/8/04/P04013, arXiv:1211.4462.

[54] CMS Collaboration, "Measurement of differential top-quark pair production cross sections in the lepton+jets channel in pp collisions at $\sqrt{s}$ = 8 TeV", Technical Report CMS-PAS-TOP-12-027, CERN, 2012.

[55] CMS Collaboration, "Measurement of the differential cross section for top quark pair production in pp collisions at $\sqrt{s}$ = 8 TeV", arXiv:1505.04480. Submitted to *Eur. Phys. J. C*.

[56] CMS Collaboration, "Measurement of W^+W^- and ZZ production cross sections in pp collisions at $\sqrt{s}$ = 8 TeV", *Phys. Lett. B* **721** (2013) 190, doi:10.1016/j.physletb.2013.03.027, arXiv:1301.4698.

[57] CMS Collaboration, "Measurement of the t-channel single-top-quark production cross section and of the $|V_{tb}|$ CKM matrix element in pp collisions at $\sqrt{s}$ = 8 TeV", *JHEP* **06** (2015) 090, doi:10.1007/JHEP06(2014)090, arXiv:1403.7366.

[58] CMS and ATLAS Collaboration, "Combination of cross-section measurements of associated production of a single top-quark and a W boson at $\sqrt{s}$ = 8 TeV with the ATLAS and CMS experiments", CMS Physics Analysis Summary CMS-PAS-TOP-14-009, ATLAS-CONF-2014-052, CERN, 2014.

[59] CMS Collaboration, "CMS Luminosity Based on Pixel Cluster Counting - Summer 2013 Update", CMS Physics Analysis Summary CMS-PAS-LUM-13-001, CERN, 2013.

[60] CMS Collaboration, "Performance of b tagging at $\sqrt{s}$ = 8 TeV in multijet, $t\bar{t}$ and boosted topology events", CMS Physics Analysis Summary CMS-PAS-BTV-13-001, CERN, 2013.

[61] A. L. Read, "Presentation of search results: the CLs technique", *J. Phys. G* **28** (2002) 2693.

[62] T. Junk, "Confidence level computation for combining searches with small statistics", *Nucl. Instrum. Meth. A* **434** (1999) 435, doi:10.1016/S0168-9002(99)00498-2, arXiv:hep-ex/9902006.